Factor Graph Optimization Based Multi-epoch Ambiguity Resolution for GNSS RTK and Its Evaluation in Hong Kong Urban Canyons

Yuan Li, *Department of Aeronautical and Aviation Engineering, the Hong Kong Polytechnic University*
Xikun Liu, *Department of Aeronautical and Aviation Engineering, the Hong Kong Polytechnic University*
Weisong Wen, *Department of Aeronautical and Aviation Engineering, the Hong Kong Polytechnic University*
Li-ta Hsu, *Department of Aeronautical and Aviation Engineering, the Hong Kong Polytechnic University*
Yilong Yuan, Tencent Technology (Beijing) Co. Ltd.
Guangyu Bian, Tencent Technology (Beijing) Co. Ltd.
Qiaoyun Chen, Tencent Technology (Beijing) Co. Ltd.

BIOGRAPHY

Yuan LI is currently a Ph.D. student at the Department of Aeronautical and Aviation Engineering, at the Hong Kong Polytechnic University. Her research interest is 3D-mapping-adied RTK/INS positioning and navigation in urban canyon environments.

Xikun Liu received his bachelor's degree in Mechanical Design, Manufacturing, and Automation from Huazhong University of Science and Technology, China in 2017, and master's degree in Mechatronics and Information Technology from Karlsruhe Institute of Technology, Germany in 2021. He is currently pursuing a Ph.D. at the Department of Aeronautical and Aviation Engineering, at the Hong Kong Polytechnic University. His research interests include GNSS and sensor-aided GNSS positioning, SLAM, and multiple sensor fusion in autonomous driving.

Dr. Weisong Wen received a Ph.D. degree in Mechanical Engineering from PolyU, in Nov 2020. He was also a visiting Ph.D. student with the Faculty of Engineering, University of California, Berkeley (UC Berkeley) in 2018. In 2020, he won the Best Presentation Award from the Institute of Navigation (ION), and the First Prize in Hong Kong Section in the Qianhai-Guangdong-Macao Youth Innovation and Entrepreneurship Competition, 2019. He is currently an Assistant Professor at PolyU. His research interests include GNSS positioning, SLAM, and collaborative positioning in challenging environments autonomous driving vehicles, and unmanned aerial vehicles.

Dr. Li-Ta Hsu is an associate professor at the Department of Aeronautical and Aviation Engineering of Hong Kong Polytechnic University. He is Limin Endowed Young Scholar in Aerospace Navigation He received his B.S. and Ph.D. degrees in Aeronautics and Astronautics from National Cheng Kung University, Taiwan, in 2007 and 2013, respectively. He was a Visiting Researcher with the Faculty of Engineering, University College London and Tokyo University of Marine Science and Technology, in 2012 and 2013, respectively. In 2013, he won a Student Paper Award and two Best Presentation Awards from the Institute of Navigation (ION). He was selected as a Japan Society

37th International Technical Meeting of the Satellite Division of the Institute of Navigation (ION GNSS+ 2024), September 16-20, 2024

https://doi.org/10.33012/2024.19805

for the Promotion of Sciences Postdoctoral Fellow with the Institute of Industrial Science, The University of Tokyo and worked from 2014 to 2016. He is an Associate Fellow in the Royal Institute of Navigation. Dr. Hsu is currently a member of ION and IEEE and serves as a member of the editorial board and reviewer in professional journals related to GNSS.

Yilong Yuan is a Research Scientist in the Tencent localization team. His research primarily concentrates on GNSS integrated navigation systems and precise positioning techniques.

Guangyu Bian is a researcher in the Tencent localization team. His primary research area focuses on positioning and navigation algorithms for mobile terminals in urban canyon environments.

Qiaoyun Chen is currently an intern in the Tencent localization team. She is pursuing her M.S. degree in Transportation Engineering at the Department of Civil Engineering, Tsinghua University. Her primary research interests include high-precision GNSS positioning and GNSS bias estimation.

ABSTRACT

With the widespread use of global navigation satellite systems (GNSS) in location-based applications, real-time kinematic (RTK) positioning has attracted much attention due to its high-precision characteristics. However, in complex environments such as urban canyons, the performance of GNSS-RTK is easily affected by insufficient and low-quality measurements, resulting in inaccurate ambiguity resolution and positioning errors of tens or even hundreds of meters. To alleviate this problem, this paper proposes a multi-epoch ambiguity resolution (AR) strategy based on factor graph optimization (FGO), and comprehensively evaluates the performance of four different AR strategies under the FGO-RTK framework. The AR strategies involved in the evaluation are: single-epoch AR without single-differenced (SD) ambiguity constraint, single-epoch AR with SD ambiguity constraint, multi-epoch AR with ambiguity merging, and our proposed method, that is, multi-epoch AR with SD ambiguity constraint. The results show that the proposed MultiSD can better utilize the temporal correlation of ambiguities across epochs, thereby improving the fixation rate and positioning accuracy in urban canyon environments. The advantages and disadvantages of the four AR strategies are validated. In short, the reliable FGO-RTK with multi-epoch AR proposed in this paper and its evaluation provide a valuable reference for the robust positioning application of GNSS in complex environments.

1 INTRODUCTION

Global Navigation Satellite Systems (GNSSs) provide globally and continuously available positioning information (Yang et al., 2020). Real-time kinematic (RTK) positioning is a vital technology for providing GNSS centimeter-level positioning services when the ambiguities of carrier phase measurements are accurately resolved. Due to its availability and accuracy, GNSS-RTK has been widely used by location-based applications, such as autonomous systems. Unfortunately, the performance of GNSS-RTK is easily hampered in challenging environments due to inadequate and low-quality measurements, particularly in urban canyons. These circumstances prevent ambiguities from accurate resolution, resulting in positioning errors of tens or even hundreds of meters (Hsu et al., 2015). The Extended Kalman Filter (EKF),

as a popular estimation algorithm for GNSS-RTK, recursively estimates the states based on prior information and current measurements, hence the positioning results can be continuously deteriorated by the dominant unhealthy observations (Takasu & Yasuda, 2009). Recently, researchers have applied Factor Graph Optimization (FGO) to GNSS to investigate robust positioning performance, because FGO can leverage the space and time correlation between multiple epochs for globally optimal estimation (Sunderhauf & Protzel, 2012; Watson & Gross, 2018). Wen & Hsu (2021) initially developed a classic FGO-RTK framework using pseudorange, carrier phase, and Doppler measurements, and demonstrated that its positioning performance surpasses that of EKF-RTK among the dense high-rise buildings in Hong Kong, but it still faces limitations in successful ambiguity resolution (AR). Therefore, achieving accurate and reliable AR for FGO-based GNSS-RTK in urban canyons remains challenging.

The common GNSS AR method, known as the ILS method, typically employs the least-squares ambiguity decorrelation adjustment (LAMBDA) algorithm to search for optimal integer solutions to ambiguities efficiently (Teunissen, 1995; Chang et al., 2005). However, in canyon environments, the ambiguity fixation rate is extremely low due to the contaminated measurements. To address this issue, external and internal information assistance are introduced. On the one hand, leveraging external information, such as visual sensors (Bai et al., 2020) or 3D city models (Ng & Hsu, 2021), Theodolite (Zhang et al., 2022), etc., can effectively help choose health measurements. However, these external information-aided approaches tend to have relatively high computational demands. On the other hand, utilizing quality indicators of GNSS raw measurements, like elevation angle and the carrier-to-noise ratio (Teunissen & Joosten, 1999; Cheng et al., 2023; Li et al., 2022; Yuan et al., 2024), to exclude poor-quality measurements is easier to implement. However, they still have certain limitations and may not fully consider unmodelled errors like multipath and non-line-of-sight errors in urban environments (Zhang et al., 2022). Interestingly, some studies use internal characteristics to impose constraints on the observation domain. Gao et al. (2022) took advantage of the time-invariant property of ambiguities that the double-differenced (DD) ambiguities are treated as constraints between adjacent epochs in the FGO-RTK framework, and the fixed integer ambiguities are used as prior information, leading to improved ambiguity fixation rate and positioning accuracy under the FGO-RTK framework in the scenario of resolving ambiguities epoch by epoch. Immediately followed, Wang et al. (2023) integrated the ambiguities from the same satellite and frequency in consecutive epochs into unified parameters if no cycle slip or interruption occurs under the sliding window-based FGO-RTK framework. Their results show that their proposed FGO-RTK framework is superior to EKF-RTK in harsh environments. This approach can improve the degree of freedom but has difficulty dealing with situations where ambiguities are incorrectly fused.

Inspired by the previous work, we want to explore whether the full use of correlations of ambiguities between multiple epochs can further improve positioning performance. Therefore, we propose a sliding window-based FGO-RTK algorithm that incorporates a multi-epoch AR method. Firstly, if no cycle slips or interruptions, the Single-differenced (SD) ambiguities are employed as a more flexible constraint between epochs (Chi et al., 2023). Secondly, all states, including positions and each ambiguity within the sliding window, are jointly solved using nonlinear optimization. Unlike the previous work, we try to extract the variance-covariance matrix of all float ambiguities in the sliding window and fix these float ambiguities using the LAMBDA method rather than just the ambiguities in the current state. Furthermore, there is a notable lack of studies evaluating and comparing AR strategies within the FGO-RTK framework under deep urban canyons. Therefore, we aim to conduct a comprehensive evaluation to assess the performance of three mainstream ambiguity strategies and our proposed method within the FGO-RTK framework in canyon environments. Our goal is to study the pros and cons of these ambiguity resolution strategies in deep urban canyon scenarios, and then provide a practical AR strategy for reliable and easily implementable applications of FGO-based real-time kinematic robust positioning in urban canyons.

This reminder of this paper is organized as follows: Section 2 presents the fundamental equations and the objective function of FGO-RTK, introduces different strategies for resolving ambiguities, and describes the flow chart of FGO-RTK. Section 3 assesses four different AR strategies and confirms their effectiveness through the analysis of one dataset gathered

in the Hong Kong urban canyons. Section 4 discusses the partial LAMBDA method and reviews the pros and cons of four AR methods. Finally, the contributions of this study are summarized, and future work is outlined.

2 METHODOLOGY

2.1 RTK based on FGO

In general, the GNSS double-difference (DD) pseudorange and carrier phase measurements are shown as follows:

$$\nabla\Delta P_{q,r,t}^{k,s} = \nabla\Delta\rho_{q,r,t}^{k,s} + \nabla\Delta I_{q,r,t}^{k,s} + \nabla\Delta T_{q,r,t}^{k,s} + \nabla\Delta E_{pr,q,r,t}^{k,s} \tag{1}$$

$$\nabla\Delta\Phi_{q,r,t}^{k,s} = \nabla\Delta\rho_{q,r,t}^{k,s} + \lambda_i\nabla\Delta N_{q,r,t}^{k,s} - \nabla\Delta I_{q,r,t}^{k,s} + \nabla\Delta T_{q,r,t}^{k,s} + \nabla\Delta E_{cp,q,r,t}^{k,s} \tag{2}$$

where ∇ and Δ denote the operators of between-satellite and between-receiver differences, respectively; superscript k and s denote the reference satellite and common satellite, respectively; subscript q and r denote the base receiver and rover receiver, respectively; subscript t denotes epoch; P and Φ denote the pseudorange and phase measurements, respectively; ρ and λ denote the receiver-satellite range and wavelength, respectively; N denote the integer ambiguity; I and T denote the ionospheric and tropospheric errors, respectively; E denotes the unmodeled errors, containing the multipath and random noise, respectively.

Under short baseline conditions, the atmospheric errors can be considered eliminated by DD measurements, and the DD measurements can be simplified as:

$$\nabla\Delta P_{q,r,t}^{k,s} = \nabla\Delta\rho_{q,r,t}^{k,s} + \nabla\Delta E_{pr,q,r,t}^{k,s} \tag{3}$$

$$\nabla\Delta\Phi_{q,r,t}^{k,s} = \nabla\Delta\rho_{q,r,t}^{k,s} + \lambda_i\nabla\Delta N_{q,r,t}^{k,s} + \nabla\Delta E_{cp,q,r,t}^{k,s} \tag{4}$$

Therefore, the error function of the DD pseudorange and carrier phase factor can be obtained as follows:

$$\left\|e_{pr,q,r,t}^{k,s}\right\|_{\Omega_{pr,q,r,t}^{k,s}}^2 = \left\|\nabla\Delta P_{q,r,t}^{k,s} - \nabla\Delta\rho_{q,r,t}^{k,s}\right\|_{\Omega_{pr,q,r,t}^{k,s}}^2 \tag{5}$$

$$\left\|e_{cp,q,r,t}^{k,s}\right\|_{\Omega_{cp,q,r,t}^{k,s}}^2 = \left\|\nabla\Delta\Phi_{q,r,t}^{k,s} - \nabla\Delta\rho_{q,r,t}^{k,s} - \lambda_i\nabla\Delta N_{q,r,t}^{k,s}\right\|_{\Omega_{cp,q,r,t}^{k,s}}^2 \tag{6}$$

where $e_{pr,q,r,t}^{k,s}$ and $\Omega_{pr,q,r,t}^{k,s}$ denote the error factor of the DD pseudorange and the corresponding variance-covariance matrix, respectively. $e_{cp,q,r,t}^{k,s}$ and $\Omega_{cp,q,r,t}^{k,s}$ denote the error factor of the DD carrier phase and the corresponding variance-covariance matrix, respectively; $\|\cdot\|^2$ denotes the Mahala Nobis distance. The Doppler frequency factor can be written as follows:

$$\left\|e_{dp,r,t}^{s}\right\|_{\Omega_{dp,r,t}^{s}}^2 = \left\|\lambda d_{r,t}^{s} - rr_{r,t}^{s}\right\|_{\Omega_{dp,r,t}^{s}}^2 \tag{7}$$

where $d_{r,t}^{s}$ denotes the Doppler frequency; $e_{dp,r,t}^{s}$ and $\Omega_{dp,r,t}^{s}$ denote the error factor of Doppler and the corresponding variance-covariance matrix, respectively; $rr_{r,t}^{s}$ denotes the expected range rate. Since motion factor can connect two epochs and time correction between multiple epochs can better be explored, the error function of the velocity factor is as follows:

$$\left\|\mathrm{e}_{dv,r,t}\right\|_{\Omega_{dv,r,t}}^2 = \left\|\boldsymbol{v}_{r,t} - \boldsymbol{v}^*_{r,t,t-1}\right\|_{\Omega_{dv,r,t}}^2 \tag{8}$$

where $v_{r,t}$ denotes the velocity of the rover station calculated by Doppler measurement; $\boldsymbol{v}^*_{r,t,t-1} = [\,(x_t - x_{t-1})/\Delta t, (y_t - y_{t-1})/\Delta t, (z_t - z_{t-1})/\Delta t]$ denotes the velocity calculated using the two position states; Δt denotes the time interval between the two coordinates for calculating the velocity; $\mathrm{e}_{dv,r,t}$ and $\Omega_{dv,r,t}$ denote the error factor of velocity and the corresponding variance-covariance matrix, respectively. Therefore, the objective function of FGO-RTK using pseudorange, carrier phase and Doppler frequency is as follows:

$$\hat{\mathrm{x}} = \underset{\mathrm{x}}{\operatorname{argmin}} \sum_{s,t} \left(\left\|e_{pr,q,r,t}^{k,s}\right\|_{\Omega_{pr,q,r,t}^{k,s}}^2 + \left\|e_{cp,q,r,t}^{k,s}\right\|_{\Omega_{cp,q,r,t}^{k,s}}^2 + \left\|e_{dp,r,t}^{s}\right\|_{\Omega_{dp,r,t}^{s}}^2 + \left\|\mathrm{e}_{dv,r,t}\right\|_{\Omega_{dv,r,t}}^2\right) \tag{9}$$

Additionally, a flexible SD ambiguity constraint can be added using the time-invariant ambiguity constraint, and the

error function can be written as follows:

$$\left\|\mathrm{e}_{sd,q,r,t}\right\|^2_{\Omega_{sd,q,r,t}} = \left\|\nabla N_{q,r,t} - \nabla N_{q,r,t-1}\right\|^2_{\Omega_{sd,q,r,t}} \tag{10}$$

where $\mathrm{e}_{sd,q,r,t}$ and $\Omega_{sd,q,r,t}$ denote the error factor of SD ambiguity constraints and the corresponding variance-covariance matrix, respectively; ∇N denotes the SD ambiguities between stations. And the corresponding objective function to be optimized is as follows:

$$\hat{\mathrm{x}} = \underset{\mathrm{x}}{\operatorname{argmin}} \sum_{s,t}\left(\left\|e^{k,s}_{pr,q,r,t}\right\|^2_{\Omega^{k,s}_{pr,q,r,t}} + \left\|e^{k,s}_{cp,q,r,t}\right\|^2_{\Omega^{k,s}_{cp,q,r,t}} + \left\|e^{s}_{dp,r,t}\right\|^2_{\Omega^{s}_{dp,r,t}} + \left\|\mathrm{e}_{dv,r,t}\right\|^2_{\Omega_{dv,r,t}} + \left\|\mathrm{e}_{sd,q,r,t}\right\|^2_{\Omega_{sd,q,r,t}}\right) \tag{11}$$

In this research, the positioning states, velocities and SD carrier ambiguities in the sliding window are estimated. If each SD ambiguity is set independently in each epoch, the unknown parameters are as follows:

$$x_t = [\boldsymbol{r}\ , \boldsymbol{v},\ \nabla \boldsymbol{N}] \tag{12}$$

where $\boldsymbol{r} = [\boldsymbol{r}_{t-n}, \dots, \boldsymbol{r}_{t-2},\ \boldsymbol{r}_{t-1}, \boldsymbol{r}_t]$ denotes all the position states in the sliding window; $\boldsymbol{v} = [v_{t-n}, \dots, v_{t-2}, v_{t-1}, v_t]$ denotes all the velocities of receivers in the sliding window; $\nabla \boldsymbol{N} = [\nabla N^1_{t-n},\ \nabla N^2_{t-n}, \dots\ \nabla N^m_{t-n}, \nabla N^1_{t-2}, \nabla N^2_{t-2}, \dots, \nabla N^m_{t-2},\ \nabla N^1_{t-1},\ \nabla N^2_{t-1}, \dots, \nabla N^m_{t-1},\ \nabla N^1_t, \nabla N^2_t, \dots, \nabla N^m_t]$ indicates all the SD ambiguities in the sliding window; m denotes the number of SD ambiguities per epoch.

If the same SD ambiguities are integrated into the unified parameters without cycle slips or interruptions, the unknown parameters are estimated:

$$x_t = [\boldsymbol{r}\ , \boldsymbol{v},\ \nabla \boldsymbol{N_M}] \tag{13}$$

where $\nabla \boldsymbol{N_M} = [\nabla N^1, \nabla N^2 \dots, \nabla N^l]$ indicates all the merged ambiguities in the sliding window; l denotes the number of merged ambiguities in the sliding window.

2.2 AR strategies

After obtaining float ambiguities through FGO, AR becomes a crucial step for achieving high-precision positioning results. Within the FGO framework, several mainstream ambiguity processing strategies exist, including attaching the SD equality constraints between epochs and merging the same ambiguities in consecutive epochs. The former fails to fully utilize the correlation between ambiguities across epochs, while the latter roughly fuses the parameters, which cannot flexibly handle the consequences of incorrect fusion.

Building on these methods, this study aims to explore a multi-epoch AR strategy based on the SD ambiguity constraint under the sliding window-based FGO-RTK framework. This approach retains the flexibility of the SD constraint while fully exploiting the temporal correlation of the ambiguity between epochs, that is, extracting the variance matrix of all float ambiguities in the sliding window and fixing these ambiguities simultaneously. Consequently, this study compares and evaluates four AR strategies, including resolving the ambiguities epoch by epoch using LAMBDA (Single), attaching SD ambiguity equality constraints between epochs and resolving ambiguities epoch by epoch using LAMBDA (SingleSD), merging the same ambiguities and resolving them together across multiple epochs using LAMBDA (MultiM), and our proposed method, that is, attaching SD ambiguity equality constraints between epochs and resolving ambiguities together across multiple epochs using LAMBDA (MultiSD). Figure 1 illustrates the factor graph of the four AR strategies in a sliding window, from left to right: Single, SingleSD, MultiM, and MultiSD. The red dashed boxes mark the ambiguities handled by the four strategies within the window, respectively. Specifically, when performing LAMBDA, the Single and SingleSD strategies extract the ambiguity and variance-covariance matrix in the current epoch, while the MultiM strategy utilizes all unified ambiguities and the corresponding variance-covariance matrix within the sliding window. Differently, the MultiSD strategy maintains a distinct extraction of each ambiguity parameter and its variance-covariance matrix within the sliding window.

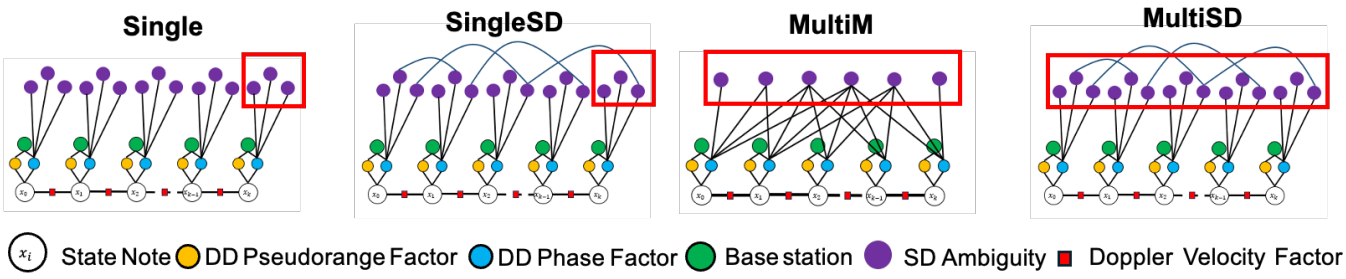

FIGURE 1 Factor graph of four AR strategies, from left to right: Single, SingleSD, MultiM, and MultiSD, respectively.

2.3 Overview of the FGO-RTK with different AR strategies

The following is a detailed description of the process:

First, the pseudorange, carrier phase, and Doppler measurements are used. The DD measurement is constructed using data from both the base station and the rover station. Then, cycle slip detection is performed to add SD ambiguities constraints or merge the same ambiguities.

Second, the DD pseudorange factor, DD carrier phase factor, Doppler measurements factor, and motion factor are constructed. The nonlinear least squares problem is solved using the Ceres solver to obtain the RTK float solution, including the position states, velocities, and SD ambiguities. Then, the float ambiguities along with their corresponding variance-covariance matrix, are extracted. The specific ambiguities extracted vary depending on the employed AR strategy, as illustrated in red boxes in Figure 1.

Third, to mitigate the impact of some contaminated measurements to improve the ambiguity fixation rate and positioning accuracy, a partial ambiguity resolution method (PAR) is introduced. Specifically, first, the ambiguities are sorted by variance and then elevation angle. Second, ambiguities with a variance greater than τ are all discarded. If the number of ambiguities exceeds δ, enter the LAMBDA part. Otherwise, a float solution is directly output. Then, a ratio test is conducted. If the ratio test is successful, a fixed solution is produced. Otherwise, the PAR strategy is employed. If LAMBDA fails, the ambiguity parameter with the highest variance or the lowest elevation angle is discarded, and then the LAMBDA method is reattempted. This process continues until the ratio test is satisfied and a fixed solution is produced, or the number of ambiguity parameters is less than δ, in which case the float solution is used directly. Figure 2 shows the flow chart of the FGO-RTK with method MultiM. The characteristic of this method is extracting and resolving all ambiguities in the sliding window together, which is filled in yellow in Figure 2.

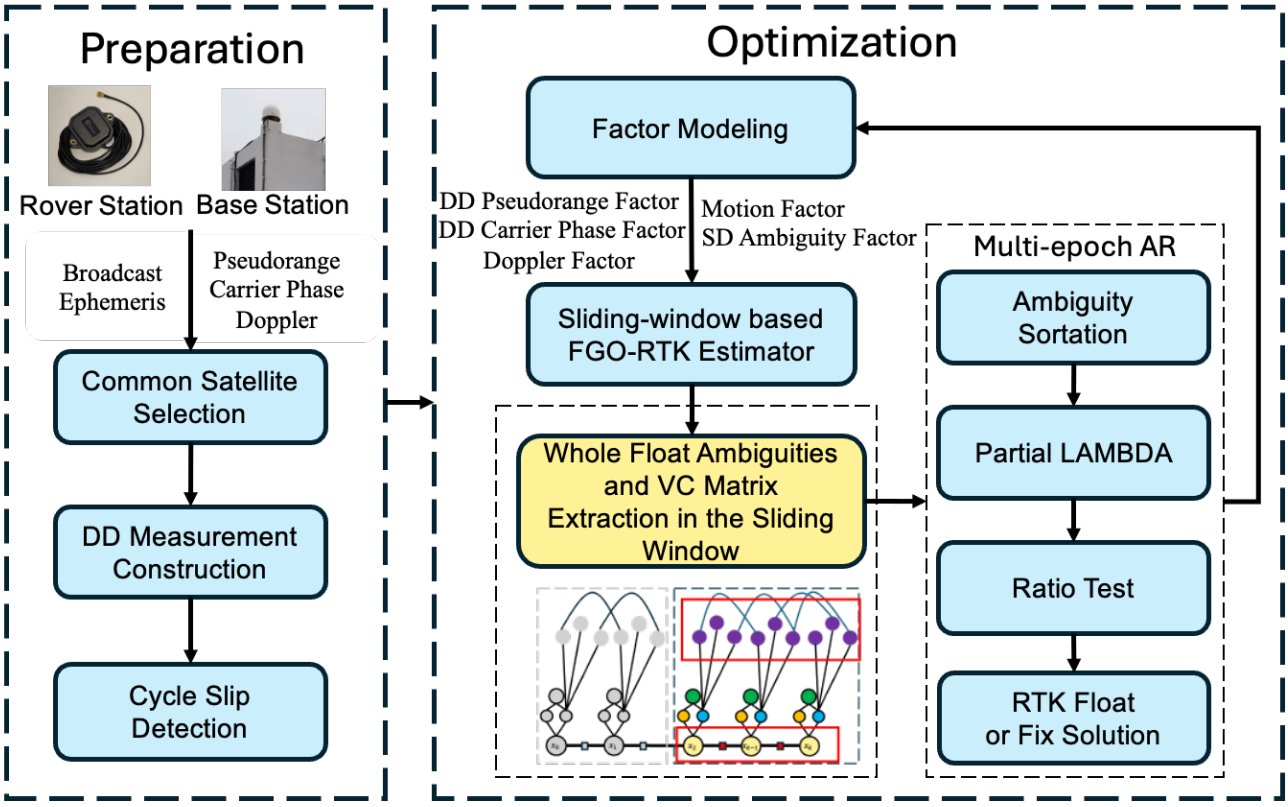

FIGURE 2 Flow chart of the FGO-RTK with method MultiM

3 URBAN KINEMATIC EXPERIMENT EVALUATION

3.1 Experimental Setup

To assess the feasibility and performance of different AR strategies for FGO-RTK positioning, an urban kinematic experiment was conducted. The dataset was collected using low-cost u-blox F9P receivers mounted on a vehicle in Kowloon Tong, Hong Kong, an area with many urban canyons. The urban canyon dataset (Canyon 1) was recorded from GPS time 3:35:00 to 3:39:00 on the 161st day of the year (DOY), with a distance of 651 meters. The dataset was gathered on urban streets enclosed by dense buildings and trees, with a sampling rate of 1Hz. Figure 3 depicts the dynamic trajectory of the Canyon 1, represented by the blue line. Then the performance of four different AR methods under the FGO-RTK framework is compared and evaluated using the Canyon 1, which is outlined below:

(1) **FGO-RTK with the Single method:** FGO-based RTK positioning using the DD pseudorange, DD carrier phase, and Doppler measurements, solving ambiguities epoch by epoch by LAMBDA

(2) **FGO-RTK with the SingleSD method:** FGO-based RTK positioning using the DD pseudorange, DD carrier phase, and Doppler measurements with SD ambiguity constraints between epochs, solving ambiguities epoch by epoch by LAMBDA

(3) **FGO-RTK with the MultiM method:** FGO-based RTK positioning using the DD pseudorange, DD carrier phase, and Doppler measurements with merging the same ambiguities, solving ambiguities among multiple epochs together by LAMBDA

(4) **FGO-RTK with the MultiSD method:** FGO-based RTK positioning using the DD pseudorange, DD carrier phase, and Doppler measurements with SD ambiguity constraints between epochs and without merging the same ambiguities, solving ambiguities among multiple epochs together by LAMBDA

FIGURE 3 Dynamic trajectories of the Canyon 1 (blue).

Table 1 gives the detailed processing strategies of FGO-RTK. The base station used is the Hong Kong base station Stonecutters Island Station (HKSC). The coordinates of the base station are accurately determined in advance by long-term measurements. The rover receiver and the HKSC form short baselines. Double-frequency measurements from GPS and BDS systems are used. The following is an explanation of some threshold settings in the implementation of FGO-RTK. If the Ratio exceeds 2.5, the ambiguities are considered successfully fixed. Cycle slip detection uses the loss of lock indicator (LLI) and geometry-free (GF) methods. If the time gap between two ambiguities from the same satellite and frequency is longer than the sampling interval, the ambiguity is seen as discontinuous. And the new ambiguity is then added as a new parameter during MultiM processing. When performing LAMBDA, ambiguities with a variance greater than 0.45 are directly eliminated. Considering the joint resolution of multi-epoch ambiguities, the minimum threshold of the number of ambiguities is not set to a fixed number but is set to 80% of the total number of ambiguities.

TABLE 1 Detailed processing strategies of FGO-RTK

Item	Strategy
Measurement type	Pseudo range, Carrier Phase, Doppler
Measurement frequency	GPS: L1, L2; BDS: B1, B2
Cut-off elevation	10°
Cut-off SNR	20 dB-Hz
Ambiguity resolution	LAMBDA
LAMBDA ratio test	2.5
Cycle slip detection	LLI, GF
Window length	3 Hz
Initial position	SPP solution

3.2 Performance Evaluation in a Canyon Environment

The performance of four AR strategies under the FGO-RTK framework in urban canyon dataset one (Canyon 1) is evaluated. The number of satellites in Canyon 1 is between 10-16, and the GDOP is between 1.5-3. The trajectories of FGO-RTK results with different AR strategies are depicted in Figure 4 from left to right: Single, SingleSD, MultiM, and MultiSD, respectively. It can be seen that the trajectory of method Single is rough. The reason may be that the ambiguity value is reinitialized for estimation at each epoch and there is no reliable prior value. The trajectories of the other three methods are relatively smooth, and the 3D RMSE accuracy of most epochs is below 4 m.

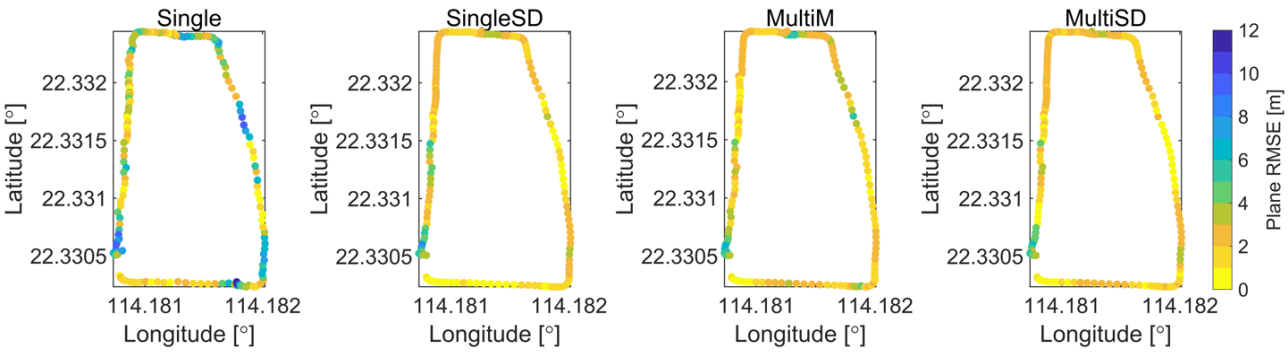

FIGURE 4 The trajectories of FGO-RTK results with different AR strategies in Canyon 1, from left to right: Single, SingleSD, MultiM, and MultiSD, respectively.

Figure 5 shows the time series of FGO-RTK positioning results with different AR strategies in Canyon 1. It can be found that the results of method Single are less stable, but not affected by the large errors from previous epochs. For example, at epochs 100-140, it outperforms the other three methods. As for method MultiM, by merging the ambiguity parameters in the sliding window, its solution is more stable than method Single. But sometimes there are big fluctuations, which may be caused by incorrect fusion, such as at epochs 160-180. In addition, the positioning results of methods SingleSD and MultiSD are smoother, and the importance of SD ambiguity constraints is mainly reflected in this way. The overall accuracy of Method MultiSD is better than method SingleSD, especially at epochs 150-180. Table 2 shows the statistics of FGO-RTK solutions with four AR strategies in the east, north, and up (ENU) frame. The terms MEAN, RMSE, and MAX represent the mean value, root mean square error, and maximum value of the positioning errors, respectively. From the statistical results in Table 2, several findings can be made. Firstly, the unconstrained method Single exhibits the worst accuracy, with a 3D RMSE of 4.596 m. Secondly, the method MultiM obtains more reliable float solutions in most epochs compared with the Single, with a 3D RMSE of 2.763 m. Thirdly, the SD ambiguity constraint can effectively improve the fixation rate, thereby improving positioning accuracy. Method SingleSD reduces the 3D RMSE to 2.528 m and increases the fixation rate by 18.1% compared with the Single. Furthermore, MultiSD has the highest fixation rate and the best positioning accuracy with a 3D RMSE of 2.312 m. Compared with the method SingleSD, its fixation rate is further improved by 7.2%, and the RMSE decreases by 0.216 m. It is worth mentioning that there are some cases where the ambiguity is falsely fixed. However, the improvement in the fixation rate of MultiSD still brings some benefits to positioning accuracy. Overall, MultiSD outperforms the other three methods both in fixation rate and accuracy.

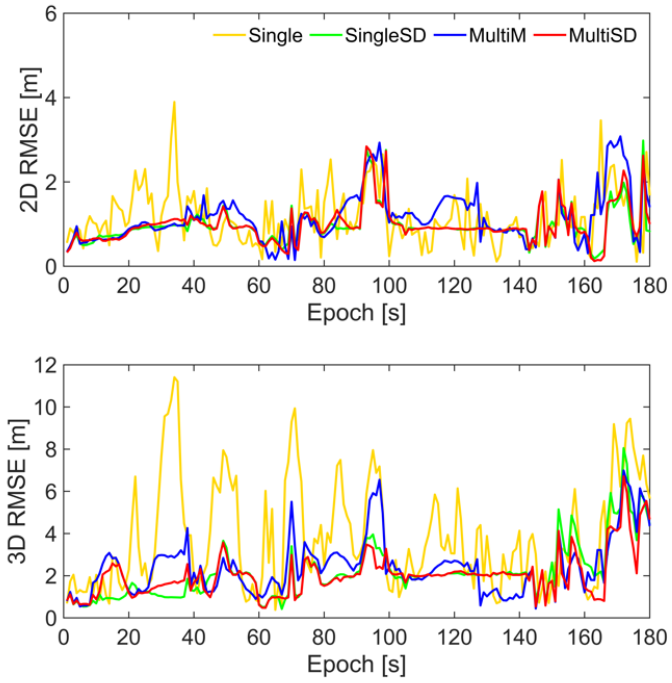

FIGURE 5 Time series of FGO-RTK positioning results with different AR strategies in Canyon 1

TABLE 2 Statistics of FGO-RTK solutions with four AR strategies in Canyon 1

AR Strategy	2D MEAN (m)	3D MEAN (m)	2D RMSE (m)	3D RMSE (m)	2D MAX (m)	3D MAX (m)	Fix rate (%)
Single	1.192	3.836	1.401	4.597	5.949	11.409	5.5
SingleSD	0.979	2.166	1.086	2.528	3.755	8.049	23.6
MultiM	1.171	2.427	1.322	2.763	3.081	6.990	0
MultiSD	0.992	2.058	1.099	2.312	3.015	6.712	30.8

4 DISCUSSIONS

4.1 The Effect of the Threshold of PAR

The following is a discussion on the impact of the threshold of PAR on the performance of the MultiSD method. We would like to further verify the reliability and rationality of the proposed method. As mentioned above, during the PAR process, a threshold is set, that is, when the number of ambiguities is lower than 80% of all ambiguities in each AR process, the PAR algorithm is stopped. Figure 6 displays the statistical results of FGO-RTK with MultiSD with different ratios. The left side of the vertical axis indicates the positioning accuracy, while the right side shows the ambiguity fixation rate. The threshold for each AR process is determined by multiplying the set ratio by the number of ambiguities. The ratio ranges from 0.4 to 1, with an interval of 0.1. It can be seen that as the threshold decreases, the fixation rate increases and the accuracy shows an upward trend. However, when the ratio is lower than 0.5, the accuracy has a clear downward trend, which means that the threshold cannot be too low. The combination of the MultiSD method and the PAR algorithm fully uses the correlation between multi-epoch ambiguities to assist in resolving these ambiguities effectively.

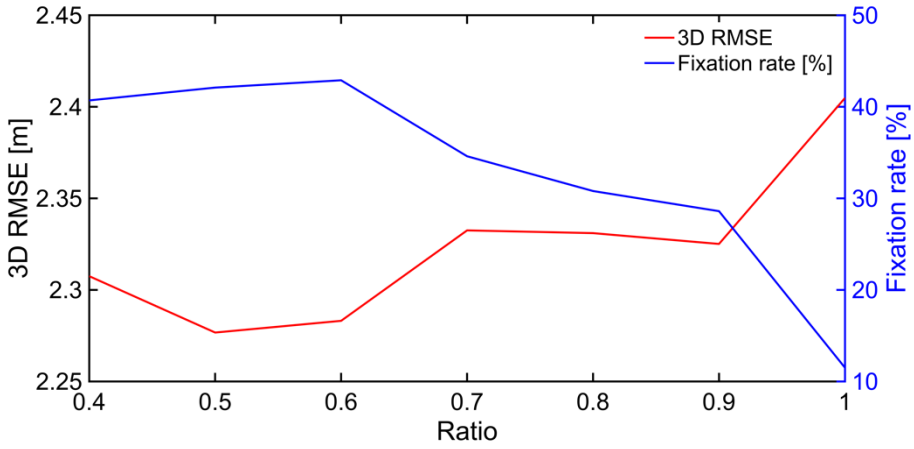

FIGURE 6 Statistical results on FGO-RTK with different ratios of PAR using MultiSD

4.2 Pros and Cons of different AR strategies

Based on the above research, this section summarizes and discusses four AR strategies. First, the Single strategy is not much affected by previous poor epochs, but its positioning error fluctuates greatly and has the worst accuracy among the four AR strategies. Second, MultiM can improve the reliability of float solutions compared with Single, but incorrect fusion can also lead to relatively large errors. Third, the SingleSD and MultiSD strategies have flexible ambiguity constraints and can improve the fixation rate and thus positioning accuracy compared to Single. However, wrong SD ambiguity constraints can degrade good positioning results. Hence, the weight of the SD ambiguity constraint can be properly adjusted if needed. So, the reason why our method MultiSD has an advantage is that it is a relatively flexible MultiM. Fourth, the MultiSD strategy can further improve the ambiguity fixation rate and positioning accuracy based on SingleSD. To conclude, MultiSD has its superiority in both static and kinematic scenarios compared with the other three methods in urban canyons.

5 CONCLUSIONS AND FUTURE WORK

At present, the pursuit of high-precision positioning in canyon environments is a hot topic. Reliable AR strategy is a prerequisite for obtaining high-precision positioning results. We propose a multi-epoch PAR method under the FGO-RTK framework. And then we comprehensively evaluate four different AR strategies within the FGO-RTK framework. The above results show that the FGO-RTK with multi-epoch AR and SD ambiguity constraints proposed in this research can make full use of the temporal correlation of ambiguities and thus better handle the low fixation rate issues in urban canyons, thereby improving positioning accuracy. Finally, the effect of the threshold of PAR is discussed, and the pros and cons of the four strategies are summarized.

Issues that need to be further explored and addressed in the future include: first, PAR can be combined with indicators that can better reflect the characteristics of urban canyons; second, the integer ambiguities often cannot be correctly resolved in urban canyons, and how to alleviate this problem requires further study; finally, if the ambiguities cannot be successfully fixed, the best integer equivariant (BIE) estimation and the suitable weight function for BIE method (Teunissen, 2003, 2020) in urban canyons can be further explored to obtain more reliable float solutions.

ACKNOWLEDGMENTS

The authors acknowledge the Smart Traffic Fund project (PSRI/73/2309/PR), GraphGNSSLib software, and GICI-Lib software.

REFERENCES

Chang, X.-W., Yang, X., & Zhou, T. (2005). MLAMBDA: A modified LAMBDA method for integer least-squares estimation. *J Geodesy*, *79*(9), 552–565. https://doi.org/10.1007/s00190-005-0004-x

Cheng, Q., Chen, W., Sun, R., & Ding, M. (2023). Strategy for Single-Epoch RTK Positioning Using Dual-Frequency in Urban Areas. *IEEE Internet Things J.*, 1–1. https://doi.org/10.1109/JIOT.2023.3300538

Chi, C., Zhang, X., Liu, J., Sun, Y., Zhang, Z., & Zhan, X. (2023). GICI-LIB: A GNSS/INS/Camera Integrated Navigation Library. *IEEE Robotics and Automation Letters*, *8*(12), 7970–7977. https://doi.org/10.1109/LRA.2023.3324825

Gao, H., Li, H., Huo, H., & Yang, C. (2022). *Robust GNSS Real-Time Kinematic with Ambiguity Resolution in Factor Graph Optimization*. 835–843. https://doi.org/10.33012/2022.18190

Hsu, L.-T., Jan, S.-S., Groves, P. D., & Kubo, N. (2015). Multipath mitigation and NLOS detection using vector tracking in urban environments. *GPS Solutions*, *19*(2), 249–262. https://doi.org/10.1007/s10291-014-0384-6

Li, Z., Xu, G., Guo, J., & Zhao, Q. (2022). A sequential ambiguity selection strategy for partial ambiguity resolution during RTK positioning in urban areas. *GPS Solut*, *26*(3), 92. https://doi.org/10.1007/s10291-022-01279-3

Sunderhauf, N., & Protzel, P. (2012). Towards robust graphical models for GNSS-based localization in urban environments. *International Multi-Conference on Systems, Sygnals & Devices*, 1–6. https://doi.org/10.1109/SSD.2012.6198059

Takasu, T., & Yasuda, A. (2009). *Development of the low-cost RTK-GPS receiver with an open source program package RTKLIB*. *1*, 1–6.

Teunissen, P. J. G. (1995). The least-squares ambiguity decorrelation adjustment: A method for fast GPS integer ambiguity estimation. *Journal of Geodesy*, *70*(1), 65–82. https://doi.org/10.1007/BF00863419

Teunissen, P. J. G. (2003). Theory of integer equivariant estimation with application to GNSS. *Journal of Geodesy*, *77*(7–8), 402–410. https://doi.org/10.1007/s00190-003-0344-3

Teunissen, P. J. G. (2020). Best integer equivariant estimation for elliptically contoured distributions. *Journal of Geodesy*, *94*(9), 82. https://doi.org/10.1007/s00190-020-01407-2

Teunissen, P. J. G., & Joosten, P. (1999). Geometry-free Ambiguity Success Rates in Case of Partial Fixing. In: *Proceedings of the 1999 national technical meeting of the institute of navigation*. pp 201–207

Wang, X., Li, X., Shen, Z., Li, X., Zhou, Y., & Chang, H. (2023). Factor graph optimization-based multi-GNSS real-time kinematic system for robust and precise positioning in urban canyons. GPS Solutions, 27(4), 200. https://doi.org/10.1007/s10291-023-01538-x

Watson, R. M., & Gross, J. N. (2018). Evaluation of kinematic precise point positioning convergence with an incremental graph optimizer. *2018 IEEE/ION Position, Location and Navigation Symposium (PLANS)*, 589–596. https://doi.org/10.1109/PLANS.2018.8373431

Wen, W., & Hsu, L.-T. (2021). Towards Robust GNSS Positioning and Real-time Kinematic Using Factor Graph Optimization. *2021 IEEE International Conference on Robotics and Automation (ICRA)*, 5884–5890. https://doi.org/10.1109/ICRA48506.2021.9562037

Yang, Y., Mao, Y., & Sun, B. (2020). Basic performance and future developments of BeiDou global navigation satellite system. *Satellite Navigation*, *1*(1), 1. https://doi.org/10.1186/s43020-019-0006-0

Yuan, H., Zhang, Z., He, X., Zeng, J., & Li, X. (2024). Resilient Ambiguity Resolution Strategy in GNSS Real-Time Kinematic Positioning for Urban Environments. *IEEE Internet of Things Journal*, 1–1. https://doi.org/10.1109/JIOT.2024.3408217

Zhang, Z., Li, Y., He, X., Chen, W., & Li, B. (2022). A composite stochastic model considering the terrain topography for real-time GNSS monitoring in canyon environments. *J Geod*, *96*(10), 79. https://doi.org/10.1007/s00190-022-01660-7